Inorg. Chem. **2006**, *45*, 3217–3223

Crystal Structure and Ionic Conductivity of Three Polymorphic Phases of Rubidium Trifluoromethyl Sulfonate, $RbSO_3CF_3$

Lars Hildebrandt, Robert Dinnebier, and Martin Jansen*

Max-Planck-Institut für Festkörperforschung, Heisenbergstrasse 1, D-70569 Stuttgart, Germany

Received September 21, 2005

The crystal structures of three polymorphic phases of rubidium trifluoromethyl sulfonate ($RbSO_3CF_3$, rubidium 'triflate') were solved from X-ray powder diffraction data. At room temperature, rubidium triflate crystallizes in the monoclinic space group *Cm* with lattice parameters of $a = 19.9611(5)$ Å, $b = 23.4913(7)$ Å, $c = 5.1514(2)$ Å, $\beta = 102.758(2)°$; $Z = 16$. At $T = 321$ K, a first-order phase transition occurs toward a monoclinic phase in space group $P2_1$ with lattice parameters at $T = 344$ K of $a = 10.3434(5)$ Å, $b = 5.8283(3)$ Å, $c = 5.1982(3)$ Å, $\beta = 104.278(6)°$; $Z = 2$). At $T = 461$ K, another phase transition, this time of second order, occurs toward an orthorhombic phase in space group *Cmcm* with lattice parameters at $T = 510$ K of $a = 5.3069(2)$ Å, $b = 20.2423(10)$ Å, $c = 5.9479(2)$ Å; $Z = 4$. As a common feature within all three crystal structures of rubidium triflate, the triflate anions are arranged in double layers with the lipophilic CF_3 groups facing each other. The rubidium ions are located between the SO_3 groups. The general packing is similar to the packing in cesium triflate. Rubidium triflate can be classified as a solid electrolyte with a specific ionic conductivity of $\sigma = 9.89 \times 10^{-9}$ S/cm at $T = 384$ K and $\sigma = 3.84 \times 10^{-6}$ S/cm at $T = 481$ K.

Introduction

Some salts with complex anions (e.g., Li_2SO_4,[1] Na_3PO_4[2−7]) show phase transitions into a dynamically disordered high-temperature phase (rotor phase) which can be accompanied by a drastic increase in the respective cationic conductivity,[8] caused by the 'volume effect',[9,10] as well as by the 'paddle-wheel mechanism'.[11] This feature makes the alkali salts of the trifluoromethyl sulfonic acid an interesting class of rotor phases according to the various degrees of rotational freedom of the triflate anion compared to, e.g., the phosphate anion.

Trifluoromethyl sulfonic acid was first synthesized in 1954[12] and became accessible in high yields by using sodium dithionite and trifluoromethyl bromide as starting materials.[13] Alkali metal salts were obtained by neutralizing the acid with barium hydroxide and an ion exchange reaction with the respective alkali metal sulfate[14] or, alternatively, by direct reaction of the acid with the respective hydroxides or carbonates.[12,15−18]

Until recently, only few crystal structures of solvent-free metal triflates were known. The distinct tendency to disordered phases at elevated temperatures makes the growths of single crystals suitable for structure determination difficult. The crystal structures of the room-temperature modifications

* To whom correspondence should be addressed. Fax: (0711) 689 1502. E-mail: M.Jansen@fkf.mpg.de.

(1) Kvist, A.; Bengtzelius, A. Fast Ion Transport in Solids. In *Solid State Batteries and Devices*; Gool, W. v., Ed.; North-Holland: New York, 1973; p 193.
(2) Wiench, D. M.; Jansen, M. *Z. Anorg. Allg. Chem.* **1980**, *461*, 101.
(3) Lissel, E.; Jansen, M.; Jansen, E.; Will, G. *Z. Kristallogr.* **1990**, *192*, 233.
(4) Wilmer, D.; Banhatti, R. D.; Funke, K.; Jansen, M.; Korus, G.; Lechner, R. E.; Fitter, J. *Electrochem. Soc. Proc.* **1997**, *PV 97−24*, 797.
(5) Funke, K.; Wilmer, D.; Banhatti, R. D.; Witschas, M.; Lechner, R. E.; Fitter, J.; Jansen, M.; Korus, G. *Mater. Res. Soc. Symp. Proc.* **1998**, *527*, 469.
(6) Wilmer, D.; Banhatti, R. D.; Fitter, J.; Funke, K.; Jansen, M.; Korus, G.; Lechner, R. E. *Physica B* **1998**, *241−243*, 338.
(7) Witschas, M.; Eckert, H.; Wilmer, D.; Banhatti, R. D.; Funke, K.; Fitter, J.; Lechner, R. E.; Korus, G.; Jansen, M. *Z. Phys. Chem.* **2000**, *214*, 643.
(8) Jansen, M. *Angew. Chem.* **1991**, *103*, 1574; *Angew. Chem., Int. Ed. Engl.* **1991**, *30*, 1547.
(9) Secco, E. A. *J. Solid State Chem.* **1992**, *96*, 366.
(10) Secco, E. A. *Solid State Ionics* **1993**, *60*, 233.
(11) Lundén, A. *Solid State Ionics* **1994**, *68*, 77.
(12) Haszeldine, R. N.; Kidd, J. M. *J. Chem. Soc.* **1954**, 4228.
(13) Tordeux, B.; Langlois, B.; Wakselman, C. *J. Org. Chem.* **1989**, *54*, 2452.
(14) Miles, M. G.; Doyle, G.; Cooney, R. P.; Tobias, R. S. *Spectrochim. Acta A* **1969**, *25*, 1515.
(15) Howells, R. D.; McCown, J. D. *Chem. Rev.* **1977**, *77*, 69.
(16) Gramstad, T.; Haszeldine, R. N. *J. Chem. Soc.* **1956**, *173*.
(17) Russel, D. G.; Senior, J. B. *Can. J. Chem.* **1980**, *58*, 22.
(18) Bonner, O. D. *J. Am. Chem. Soc.* **1981**, *103*, 3262.

10.1021/ic0516313 CCC: $33.50
Published on Web 03/21/2006

of lithium,[19,20] sodium,[21] potassium,[22] and cesium triflate,[23] as well as the mixed-phase $LiRb_2SO_3CF_3$,[24] were solved from either single-crystal intensity data or high-resolution X-ray powder diffraction data. The crystal structures of the high-temperature modifications of lithium[25] and cesium triflates[23] have been determined from temperature-dependent high-resolution synchrotron powder diffraction measurements. The crystal structures of mercury(I) triflate[26] and of some divalent metal triflates $M(SO_3CF_3)_2$ (with M = Mg, Ca, Ba, Zn, Cu)[27] were published recently.

In addition to the structural studies, the dynamics of the triflate molecules, as well as the ionic conductivity of the alkali triflates, has been studied. The cationic mobility in lithium,[28] sodium,[21] potassium,[22] and cesium triflate[23] was determined by impedance spectroscopy. Solid-state NMR studies on lithium triflate have confirmed a strong correlation between the rotational motion of the anion and the translational motion of the lithium cations.[28−31] The phase diagram of the quasi-binary system $LiSO_3CF_3/RbSO_3CF_3$ was examined, and the mixed phases were investigated by solid-state NMR techniques, X-ray powder diffraction, and ionic conductivity measurements.[28]

In this paper, we present the crystal structure, the thermal behavior, the infrared spectrum, and ac conductivity of rubidium triflate.

Experimental Section

Synthesis. $RbSO_3CF_3$ was prepared by reacting diluted trifluoromethyl sulfonic acid (98% Aldrich, 0.3 M) with rubidium hydroxide. Excess acid and water were distilled off. The residue was recrystallized twice from purified water and dried in a vacuum (10^{-3} mbar) for 2 days at $T = 400$ K. The purity of the resulting white powder was checked with X-ray powder diffraction and EDX analysis. For the growing of single crystals, the compound was melted (mp = 517 K) and cooled to room temperature slowly (0.5 K/min).

X-ray Diffractometry. Single crystals of $RbSO_3CF_3$ were measured on a single-crystal diffractometer (Bruker AXS, SmartCCD). Initial atomic parameters were found by direct methods (SHELXS-97[32]), with *Cm* as the most probable space group. However, due to the poor quality of the crystal, a subsequent refinement (SHELXL-97[33]) did not converge to an acceptable *R* value. Therefore, the structural model was validated by Rietveld refinement using high-resolution X-ray powder diffraction data (D-8, Bruker, Cu $K\alpha_1$ radiation from primary Ge(111) Johanson-type monochromator; Våntag-1 position sensitive detector). The pattern was recorded in Debye−Scherrer geometry with the sample sealed in a lithium borate glass capillary of 0.5 mm diameter (Hilgenberg, glass No. 50). Data were taken in steps of 0.017° 2θ for 0.05°/min. For better statistics, the sample was spun during the measurement.

The peak profiles and precise lattice parameters were determined by LeBail-type fits[34] using the GSAS program.[35] The structural model from the single-crystal determination in space group *Cm* was validated by Rietveld refinement[36] using soft constraints for the

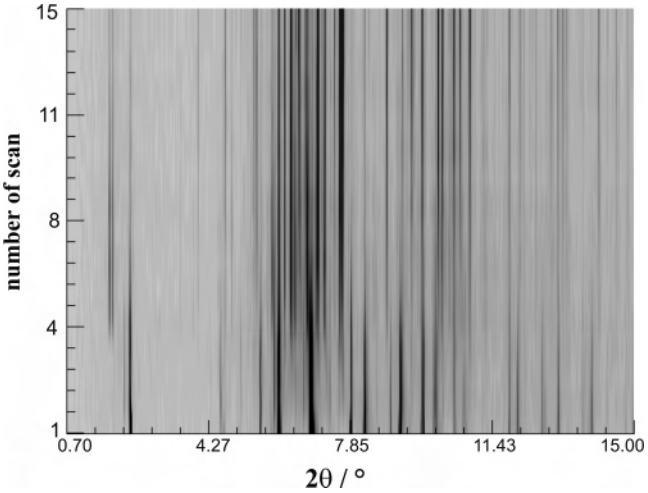

Figure 1. High-resolution synchrotron powder diffraction pattern.

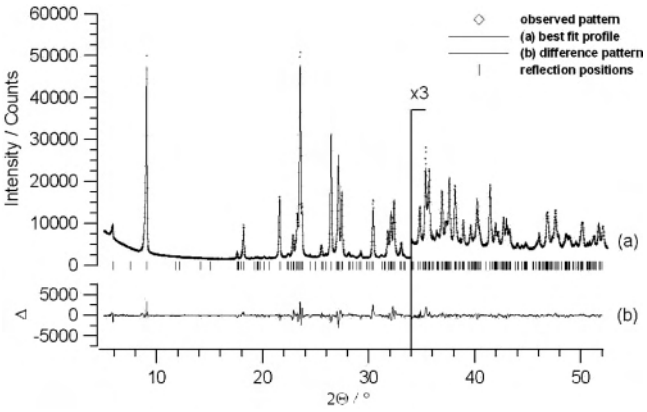

Figure 2. Scattered X-ray intensities for α-$RbSO_3CF_3$ at $T = 298$ K as a function of the diffraction angle 2θ. Shown are the observed patterns (diamonds), the best Rietveld-fit profiles (line), and the difference curve between observed and calculated profiles (below in an additional window). Intensities of the high angle part are enlarged by a factor of 3.

(19) Tremayne, M.; Lightfoot, P.; Mehta, M. A.; Bruce, P. G.; Harris, K. D. M.; Shankland, K.; Gilmore, C. J.; Bricogne, G. *J. Solid State Chem.* **1992**, *100*, 191.
(20) Bolte, M.; Lerner, H. W. *Acta Crystallogr., Sect. E: Struct. Rep. Online* **2001**, *57*, m231.
(21) Sofina, N.; Peters, E.-M.; Jansen, M., *Z. Anorg. Allg. Chem.* **2003**, *629*, 1431.
(22) Korus, G.; Jansen, M. *Z. Anorg. Allg. Chem.* **2001**, *627*, 1599.
(23) Hildebrandt, L.; Dinnebier, R.; Jansen, M. *Z. Anorg. Allg. Chem.* **2005**, *631*, 1660.
(24) Pompetzki, M.; Friese, K.; Jansen, M. *Acta Crystallogr. C* **2003**, *59*, 117.
(25) Dinnebier, R. E.; Sofina, N.; Jansen, M. *Z. Anorg. Allg. Chem.* **2004**, *630*, 1613.
(26) Rosdahl, J.; Persson, I.; Kloo, L.; Stahl, K. *Inorg. Chim. Acta* **2004**, *357*, 2624.
(27) Dinnebier, R.; Sofina, N.; Hildebrandt, L.; Jansen, M. *Acta Crystallogr. B* **2006**, submitted for publication.
(28) Pompetzki, M.; van Wüllen, L.; Jansen, M. *Z. Anorg. Allg. Chem.* **2004**, *630*, 484.
(29) van Wüllen, L.; Hildebrandt, L.; Jansen, M. *Solid State Ionics* **2005**, *176*, 1449.
(30) Mortimer, M.; Moore, E. A.; Williams, M. A. K. *J. Chem. Soc., Faraday Trans.* **1992**, *88*, 2393.
(31) Mortimer, M.; Moore, E. A.; Williams, M. A. K. *J. Chem. Soc., Faraday Trans.* **1996**, *92*, 5043.
(32) Sheldrick, G. M. *SHELXS-97 Programm zur Lösung von Kristallstrukturen*; University of Göttingen: Göttingen, Germany, 1997.
(33) Sheldrick, G. M. *SHELXL-97 Programme zur Verfeinerung von Kristallstrukturen*; University of Göttingen: Göttingen, Germany, 1997.
(34) Le Bail, A.; Duroy, H.; Fourquet, J. L. *Mater. Res. Bull.* **1988**, *23*, 447.
(35) Larson, A. C.; von Dreele, R. B. *GSAS 1994; Version 2002*; Los Alamos National Laboratory Report LAUR 86-748, 2002.
(36) Rietveld, H. M., *J. Appl. Crystallogr.* **1969**, *2*, 65.

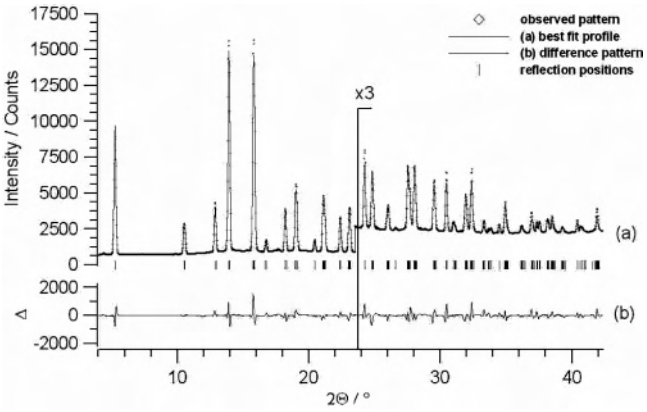

Figure 3. Scattered X-ray intensities for β-$RbSO_3CF_3$ at $T = 344$ K as a function of the diffraction angle 2θ. Shown are the observed patterns (diamonds), the best Rietveld-fit profiles (line), and the difference curve between observed and calculated profiles (below in an additional window). Intensities of the high angle part are enlarged by a factor of 3.

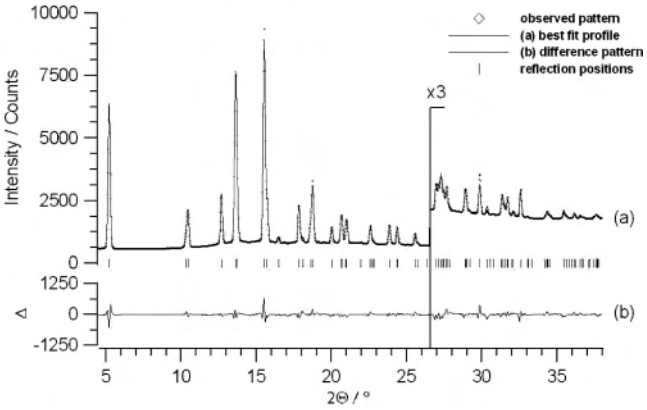

Figure 4. Scattered X-ray intensities for γ $-RbSO_3CF_3$ at $T = 510$ K as a function of the diffraction angle 2θ. Shown are the observed patterns (diamonds), the best Rietveld-fit profiles (line) and the difference curve between observed and calculated profiles (below in an additional window). Intensities of the high angle part are enlarged by a factor of 3.

bond lengths (C−F, S−O, S−F) and bond angles (O−S−O, F−C−F, O−S−C, F−C−S) to stabilize the refinement of the triflate molecule.

In situ X-ray powder diffraction data of rubidium triflate at high temperatures were taken in transmission with a small environment cell for real-time studies on a motorized goniometer head at beamline ×7B at the National Synchrotron Light Source (NSLS) at Brookhaven National Laboratory. As detector, a MAR 345 image plate reader was set up perpendicular to the beam path at a distance of approximately 170 mm from the sample. LaB_6 was used as an external standard to determine the beam center, sample-to-detector distance, exact wavelength ($\lambda = 0.9224$ Å), and tilting angle of the image plate. The sample was contained in a 0.5 mm lithium borate glass capillary loaded in a 0.8 mm sapphire capillary attached to a flow−reaction cell, similar to those described by Parise et al.[37] and Chupas et al..[38] The temperature was monitored and controlled by a 0.010 in. thermocouple (Omega) which was inserted straight into the sapphire tube adjacent to and contacting the sample capillary. The sample was aligned such that the sample closest to the thermocouple was in the X-ray beam path. The sample was heated in the temperature range from room temperature up to 523 K at 1 K/min with a small resistance heater wrapped around the sapphire tube. During exposure, the samples were rocked for 80° in order to improve randomization of the crystallites. The exposure time was 180 s plus 80 s for the readout of the image plate. Integration of the full-circle powder patterns was performed using the program FIT2D,[39,40] resulting in diagrams of corrected intensities versus the scattering angle 2θ. Any reflections due to the single-crystal sapphire capillary were excluded.

Data reduction on all powder diffraction patterns was performed using the program Powder3D.[41] Indexing of the powder pattern at $T = 344$ K led to a primitive monoclinic unit cell for β-$RbSO_3CF_3$. The extinction rules indicated $P2_1$ and $P2_1/m$ as the most probable space groups. The number of formula units per unit cell was calculated to be $Z = 2$ from volume increments. At $T = 510$ K, an orthorhombic unit cell with twice the volume of the monoclinic cell at $T = 344$ K ($Z = 4$) was found for γ-$RbSO_3CF_3$. The extinction rules, as well as the similarity to the β-$CsSO_3CF_3$, led to the most probable space groups $Cmc2_1$ or $Cmcm$.

The crystal structures of both high-temperature phases of rubidium triflate were solved using the DASH structure solution package.[42] The powder patterns at $T = 344$ and 510 K were subjected to Pawley refinements.[43] Good fits to the data were

Table 1. Crystallographic Data for α-, β-, and γ-rubidium Triflate[a]

formula	α-$RbSO_3CF_3$	β-$RbSO_3CF_3$	γ-$RbSO_3CF_3$
temp (in K)	298	344	510
fw (in g/mol)	234.53	234.53	234.53
space group	*Cm*	$P2_1$	*Cmcm*
Z	16	2	4
a (in Å)	19.9611(5)	10.3434(5)	5.3069(2)
b (in Å)	23.4913(7)	5.8283(3)	20.242(1)
c (in Å)	5.1514(2)	5.1982(3)	5.9479(3)
β (in °)	102.758(2)	104.278(6)	-
V (in $Å^3$)	2355.9(2)	303.69(2)	638.95(5)
ρ_{calc}d (in gm/cm^3)	2.645	2.565	2.438
wavelength (in Å)	1.54059	0.9224	0.9224
capillary diameter (in mm)	0.5	0.5	0.5
$R - p$ (in %)*	5.10	3.76	2.67
$R - wp$ (in %))*	7.03	5.23	3.60
$R - F^2$(in %)*	5.74	6.50	8.87
no. reflns	289	210	90

[a] Further details of the crystal structure investigation are available from the Fachinformationszentrum Karlsruhe, D-76344 Eggenstein-Leopoldshafen (Germany), on quoting the depository number CSD-415816 (α-$RbSO_3CF_3$), −415817 (β-$RbSO_3CF_3$) or −415818 (γ-$RbSO_3CF_3$), the name of the authors, and citation of the paper. [b] $R - p$, $R - wp$, and $R - F^2$ as defined in GSAS.[35]

Table 2. Selection of Intra- and Intermolecular Distances (in Å) and Angles (in deg) in α- and β-$RbSO_3CF_3$

formula	α-$RbSO_3CF_3$	β-$RbSO_3CF_3$
S−C	1.755−1.808	1.807
S−O	1.416−1.428	1.481−1.492
C−F	1.293−1.366	1.263−1.343
∠O−S−O	108.9−109.0	109.4−109.5
∠F−C−F	108.7−109.3	109.4−109.5
∠C−S−O	109.8−110.1	109.4−109.6
∠S−C−F	109.8−110.1	109.4−109.5

(37) Parise, J. B.; Cahill, C. L.; Lee, Y. J. *Can. Mineral.* **2000**, *38 N 4*, 777.
(38) Chupas, P. J.; Ciraolo, M. F.; Hanson, J. C.; Grey, C. P. *J. Am. Chem. Soc.* **2001**, *123*, 1694.
(39) Hammersley, A. P. *ESRF Internal Report, ESRF97HA02T*; European Synchroton Radiation Facility: Grenoble Cedex, France, 1997.
(40) Hammersley, A. P. *ESRF Internal Report, ESRF98HA01T*; European Synchroton Radiation Facility: Grenoble Cedex, France, 1998.
(41) Hinrichsen, B.; Dinnebier, R. E.; Jansen, M. *Z. Kristallogr.* **2005**, in press.
(42) David, W. I. F.; Shankland, K.; Shankland, N. *Chem. Commun.* **1998**, 931.
(43) Pawley, G. S. *J. Appl. Crystallogr.* **1981**, *14*, 357.

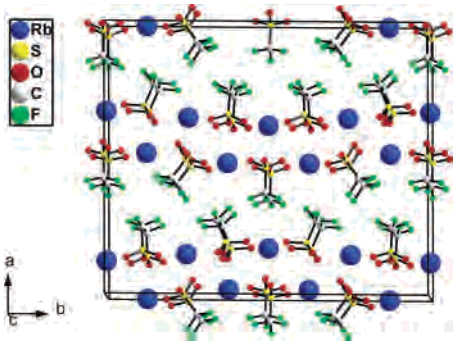

Figure 5. Crystal structure of α-$RbSO_3CF_3$ in a view along [001].

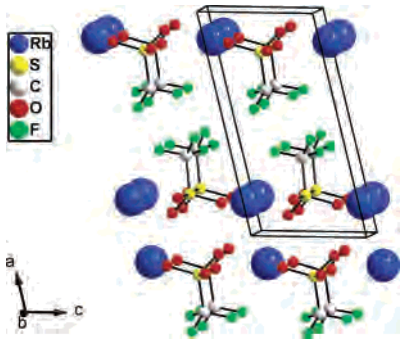

Figure 6. Crystal structure of β-$RbSO_3CF_3$ in a view along [010].

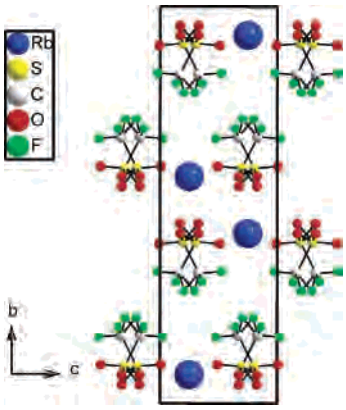

Figure 7. Crystal structure of γ-$RbSO_3CF_3$ in a view along [100]. The triflate molecules are 2-fold disordered.

obtained. An internal coordinate description of the triflate anion was constructed using bond lengths, angles, and torsion angles from corresponding lithium triflate.[19] The position of the rubidium cation, as well as the position and orientation of the triflate anion in the unit cell, were postulated. The trial structures were subjected to a global optimization where the external degrees of freedom were the positions of the rubidium cations and the triflate anions, and four-quarternions [44] describing the orientation of the molecule. The structures giving the best fit by Rietveld refinement [36] of the fractional coordinates obtained at the end of the simulated annealing run were in space group $P2_1$ for β-$RbSO_3CF_3$ and in space group *Cmcm* for γ-$RbSO_3CF_3$. As well as for the room-temperature modification, the refinement was stabilized by soft constraints for the bond lengths (C−F, S−O, S−F) and bond angles (O−S−O, F−C−F, O−S−C, F−C−S).

Low-temperature X-ray powder diffraction patterns were performed on a two-circle diffractometer (StadiP, Stoe, Cu $K\alpha_1$ radiation from primary Ge(111) Johanson-type monochromator) equipped with a 600 Series Oxford Cryosystem cold air blower. Silicon was used as external calibration standard. The lattice parameters of α-$RbSO_3CF_3$ at lower temperatures were determined by LeBail-type fits using the GSAS program.

It is worth mentioning that, during the exposure with high-resolution synchrotron radiation (ID31 of the European Synchrotron Radiation Facility (ESRF), $\lambda = 0.40009$ Å), a radiation-induced, irreversible phase transition from α-$RbSO_3CF_3$ toward a yet-unknown phase rapidly occurs in a short time, depending on the photon flux (typically in the order of <30 s) (Figure 1).

Impedance Spectroscopy. The ionic conductivity was determined using ion-blocking gold electrodes and compact polycrystalline powder samples (diameter 6 mm, thickness 0.85 mm, pressed with 350 MPa). During the measurement, the sample was placed

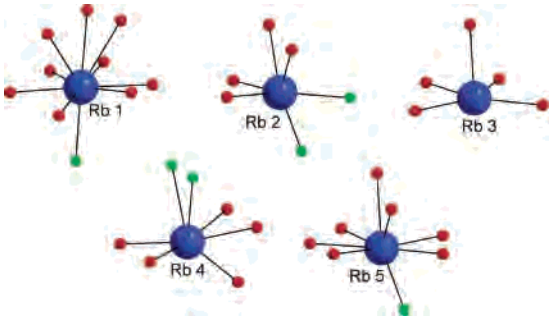

Figure 8. Coordination of the five different rubidium ions in α-$RbSO_3CF_3$.

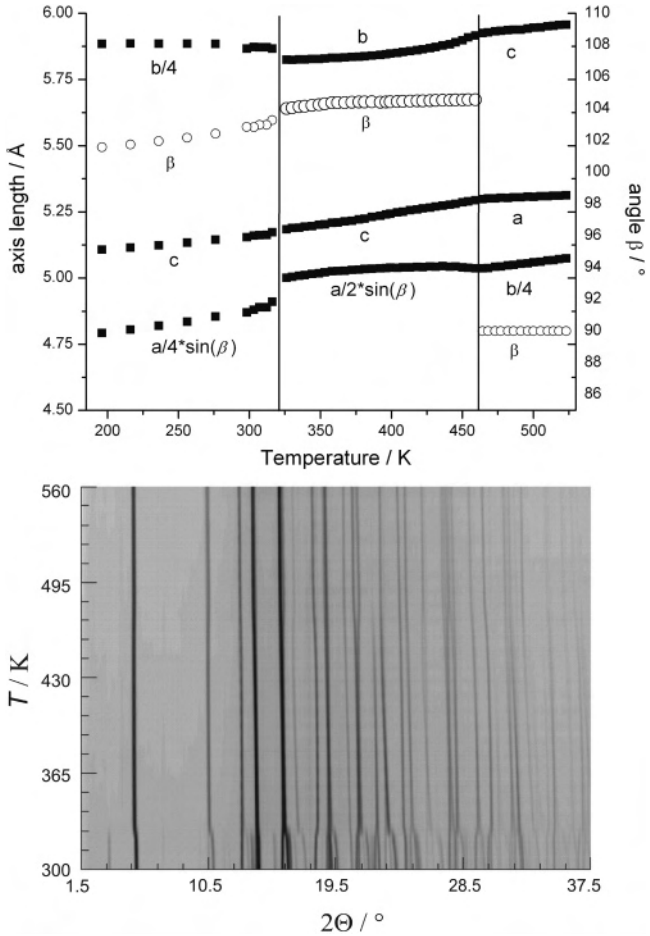

Figure 9. Lattice parameters (top) and powder diffraction pattern (bottom) of $RbSO_3CF_3$ as a function of temperature.

(44) Leach, A. R. In *Molecular Modelling − Principles and Applications*; Addison-Wesley Longman: Edinburgh Gate, Harlow, UK, 1996.

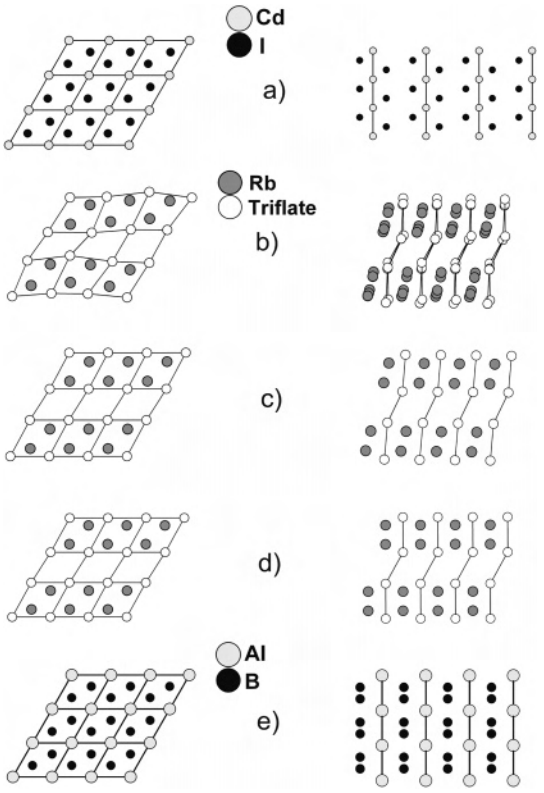

Figure 10. Crystal packings of (a) CdI_2, (b) α-$RbSO_3CF_3$, (c) β-$RbSO_3CF_3$, (d) γ-$RbSO_3CF_3$, and (e) AlB_2 with the triflate molecules drawn as balls around their center of gravity locations in two projections: [010] (left) and [001] (right) for α-and β-$RbSO_3CF_3$ and [001] (left) and [100] (right) for γ-$RbSO_3CF_3$, AlB_2 and CdI_2.

in a quartz glass cell[45] under dry argon. The temperature-dependent AC impedance spectra were measured with a Novocontrol Alpha-A 4.2 Analyzer combined with the impedance interface ZG4 in a 2-wire arrangement in a frequency range of $\nu = 0.1$ Hz to 20 MHz. Measurement and data recording were performed with the WinDETA program.[46] The bulk conductivity was determined by nonlinear mean-square deviation curve fitting of the impedance spectrum using the WinFIT program.[47]

Infrared Spectroscopy. The IR spectroscopy was performed employing a Bruker IFS 113v FTIR spectrometer. The sample was pressed to a pellet (ca. 1 mg of substance in 300 mg of KBr).

Results and Discussion

Crystal Structure. The crystal structure of α-$RbSO_3CF_3$ (*Cm*, $Z = 16$, $T = 298$ K) was solved by the combined analysis of X-ray single crystal and high-resolution X-ray powder diffraction data (Figure 2). The crystal structures of β-$RbSO_3CF_3$ ($P2_1$, $Z = 2$, $T = 344$ K) and γ-$RbSO_3CF_3$ (*Cmcm*, $Z = 4$, $T = 510$ K) have been determined from temperature-dependent synchrotron powder diffraction data (Figures 3 and 4). The lattice parameters and the agreement factors (*R* values) are listed in Table 1. A selection of inter- and intramolecular distances and angles in α- and β-$RbSO_3CF_3$ is given in Table 2. Due to the high degree of disorder in the high-temperature γ-phase of $RbSO_3CF_3$, individual bond lengths and angles are not discussed for this modification.

Table 3. Comparison of the Ideal CdI_2- and the Ideal AlB_2-Type Structure with α-, β- and γ-$RbSO_3CF_3$, with the Triflate Molecules Substituted by Their Barycenters[a]

	CdI_2	α-$RbSO_3CF_3$	β-$RbSO_3CF_3$	γ-$RbSO_3CF_3$	AlB_2
δ (in °)	120	110.8−125.0	122	120.5	120
ϵ (in °)	180	152.5−158.0	159.4	150.5	180
z_1	1/4	0.420−0.459	0.450	1/2	1/2
z_2	3/4	0.541−0.580	0.550	1/2	1/2

[a] δ defines the hexagonal angle in the projection of [010] for the α- and the β-phase and in [001] for the γ-phase, CdI_2 and AlB_2. ϵ defines the angle of the shift of the double layers in the projection along [001] for the α- and the β-phase and in [100] for the γ-phase, CdI_2 and AlB_2. z_1 and z_2 define the fractional coordinates of the cations in the hexagonal cell in the *b* direction for the α- and the β-phase and in the *c* direction for the γ-phase, CdI_2, and AlB_2.

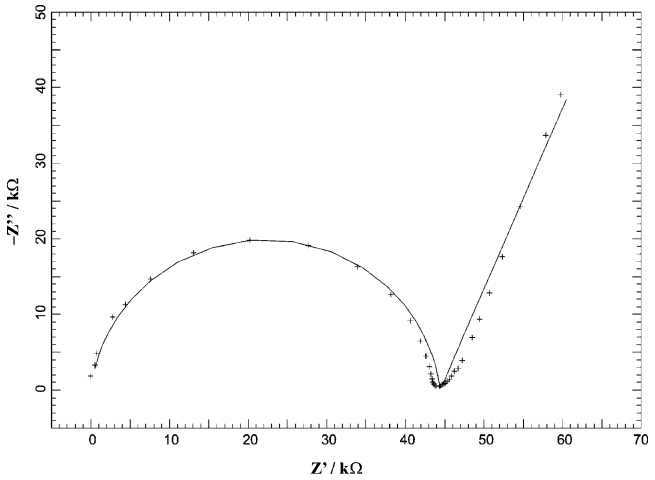

Figure 11. Impedance data for rubidium triflate presented in the complex plane format, $-Z''$ (imaginary part) vs Z' (real part) at $T = 489$ K. The equivalent circuit used to fit (line) the measured data (crosses) represents a series combination of bulk and sample−electrode interface impedance.

As it is known for all other alkali triflates, with the exception of potassium triflate, the crystal structures of α- (Figure 5), β- (Figure 6), and γ-$RbSO_3CF_3$ (Figure 7) consist of double layers of trifluoromethyl sulfonate anions with the lipophilic CF_3 groups facing each other. The conformation of the triflate anions is staggered. The rubidium ions are located between the SO_3 groups of the triflate double layers. In contrast to the β- and the γ-phase, where the triflate double layers are planar, the double layers in α-$RbSO_3CF_3$ are corrugated to form troughs and nodes. Therefore, the room-temperature modification of $RbSO_3CF_3$ shows similarities to the crystal structure of KSO_3CF_3, where the troughs are truncated to form isolated pipes.[22] In α-$RbSO_3CF_3$, the cations are not only coordinated by oxygen but also by fluorine ions (Figure 8). At $T = 321$ K, a first-order phase transitions from α-$RbSO_3CF_3$ to β-$RbSO_3CF_3$ and at $T = 461$ K, a probably second-order phase transition, according to the constant change of the volume, from β-$RbSO_3CF_3$ to γ-$RbSO_3CF_3$ (Figure 9), occur. The transformation matrixes for the unit cell parameters are given by ((1/2) 0 0; 0 (1/4) 0; 0 0 1) from the α- to the β-phase and by (0 0 $\bar{1}$; $\bar{2}$ 0 $\bar{1}$; 0 1 0) from the β- to the γ-phase.

(45) Altomare, A.; Cascarano, G.; Giacovazzo, C.; Guagliardi, A.; Moliterni, A. G. G.; Burla, M. C.; Polidori, G.; Camilli, M.; Spagna, R. *SIR97 − a Package for Crystal Structure Solution by Direct Methods and Refinement;* Computer Program, Dip. Geomineralogico: University of Bari, Italy, 1997.
(46) *Novocontrol WinDeta*, 4.5; GmbH: Hundsangen, 1995−2003.
(47) *Novocontrol WinFit*, 2.9; GmbH: Hundsangen, 1996.

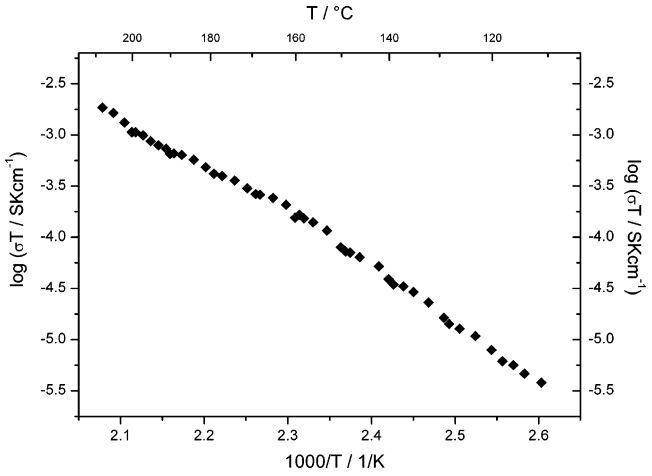

Figure 12. Arrhenius plot of the temperature-dependent bulk ionic conductivity of rubidium triflate.

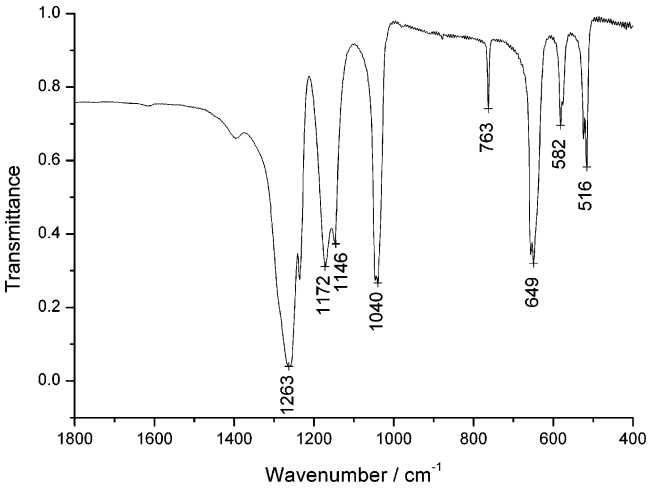

Figure 13. Infrared spectrum of α-$RbSO_3CF_3$.

β-$RbSO_3CF_3$ is isotypic to the room-temperature modification of $CsSO_3CF_3$, while γ-$RbSO_3CF_3$ is isostructural to β-$CsSO_3CF_3$.[23] As it was observed for the high-temperature phase of $CsSO_3CF_3$, the triflate molecules in γ-$RbSO_3CF_3$ are disordered. The Rietveld refinement using the ordered molecules did not converge satisfactorily. The best result was achieved for a 2-fold disordered triflate anion. Recent studies on the dynamic processes in $LiSO_3CF_3$[29] and $NaSO_3CF_3$[48] using temperature-dependent NMR measurements revealed an isotropic reorientation of the triflate molecule around its center of gravity at elevated temperatures. Regarding the disordered triflate molecule in γ-$RbSO_3CF_3$, an analogous dynamic process can be expected.

To understand the principles of crystal packing and to compare the crystal structures of the three modifications of rubidium triflate, the triflate molecules are replaced by their barycenters, X. Similarly to the crystal packing in $CsSO_3CF_3$, the rubidium triflate in the α- and β-phase form two-dimensional sheets$_\infty^2$[XRb_2] in a strongly distorted CdI_2-type structure ($P\bar{3}m1$; Cd: 0 0 0; I: 1/3 2/3 1/4). The triflate molecules are located on the cadmium sites (Figure 10), while the rubidium cations are placed on the iodine positions but shifted in *z* direction in comparison to an ideal CdI_2-type structure. The degree of distortion from an ideal hexagonal layer is decreasing with growing temperature. From the α- to the β-phase, the number of crystallographically distinguishable positions for both the rubidium cations and the barycenters of the triflate molecules reduces from five down to one. In the γ-phase, $RbSO_3CF_3$ forms separate layers in an AlB_2-type structure ($P(6/m)(2/m)(2/m)$; Al: 0 0 0; B: 1/3 2/3 1/2). The differences in the crystal packing of the different polymorphs of rubidium triflate are mostly determined by the space requirements and the (temperature dependent) sphericity of the disordered triflate molecules. In contrast to the ideal CdI_2- or AlB_2-type structure, only double layers, which are formed by the SO_3-groups of the triflate molecules, are filled with rubidium cations, while the space between the CF_3 groups is empty. The individual layers are shifted compared to the next parallel CdI_2- or AlB_2-type layer, leading to a corrugated structure of the hexagonal layers. The difference from the ideal hexagonal angle of 120° in CdI_2 decreases from α- to β-$RbSO_3CF_3$ and from β- to γ-$RbSO_3CF_3$ (Table 3).

Ionic Conductivity. Up to $T = 433$ K, the impedance data of $RbSO_3CF_3$ in the complex plane format shows only one semicircle which can be interpreted as a parallel *RQ* element (*Q*: constant phase element) in the equivalent circuit. At higher temperatures, an additional low-frequency 'spike' appears, representing the barrier to charge transfer between the sample and the ion-blocking gold electrodes (Figure 11). Therefore, the equivalent circuit has to be expanded by another constant phase element, Q_{el}, in series to the *RQ* element. The capacitance, *C*, can be determined as $C = Q^{1/n} \cdot R^{(1/n)-1}$. The calculated values for the semicircles at different temperatures ($C \approx 4 \times 10^{-12}$ F) are typical for the bulk capacitance of a sample,[49] and therefore, the semicircle can be associated with the rubidium ion conductivity in the bulk.

According to the classification by Tuller and Moon,[50] rubidium triflate may be regarded as a solid electrolyte (10^{-10} S/cm > σ > 10^{-5} S/cm). The specific ionic conductivity of the bulk amounts to $\sigma = 9.89 \times 10^{-9}$ S/cm at $T = 384$ K and $\sigma = 3.84 \times 10^{-6}$ S/cm at $T = 481$ K, which is in the same range as the conductivity of potassium triflate[22] and much higher than the conductivity of Rb_2SO_3 ($\sigma = 1.40 \times 10^{-8}$ S/cm at $T = 555$ K.[51] Both the rubidium and the potassium triflate are better ionic conductors than the lighter alkali triflates $LiSO_3CF_3$[28] and $NaSO_3CF_3$[21] at similar temperatures, which is caused by the higher polarizability of the heavier elements. The best conductivity of salts of the first main group elements is performed by the cesium triflate,[23] which can be regarded as a fast ionic conductor at high temperatures (T > 475 K.). The temperature-dependent bulk ionic conductivity of $RbSO_3CF_3$ is plotted in an Arrhenius type of diagram (Figure 12). The activation energy

(48) van Wüllen, L.; Sofina, N.; Jansen, M. *Chem. Phys. Chem.* **2004**, *5*, 1906.

(49) Irvine, J. T. S.; Sinclair, D. C.; West, A. R. *Adv. Mater.* **1990**, *2*, 132.
(50) Tuller, H. L.; Moon, P. K. *Mater. Sci. Eng. B* **1988**, *1*, 171.
(51) Gundusharma, U. M.; Secco, E. A. *Can. J. Chem.* **1987**, *65*, 1205.

of E_a = 96.0 kJ/mol was derived from the slope of the conductivity curve.

Infrared Spectroscopy. The infrared spectrum of $RbSO_3CF_3$ (Figure 13) is in good agreement with earlier publications regarding the absorption bands of the triflate molecule.[14]

Supporting Information Available: X-ray crystallographic data in cif format. This material is available free of charge via the Internet at http://pubs.acs.org.

IC0516313